

# Comparative Analysis of Mitochondrial Proteome Reveals the Mechanism of Enhanced Ram Sperm Motility Induced by Carbon Ion Radiation After In Vitro Liquid Storage

Dose-Response:  
An International Journal  
January-March 2019:1-13  
© The Author(s) 2019  
Article reuse guidelines:  
sagepub.com/journals-permissions  
DOI: 10.1177/1559325818823998  
journals.sagepub.com/home/dos



Yuxuan He<sup>1</sup>, Hongyan Li<sup>2,3,4</sup>, Yong Zhang<sup>1</sup>, Junjie Hu<sup>1</sup>, Yulong Shen<sup>1</sup>, Jin Feng<sup>1</sup>, and Xingxu Zhao<sup>1</sup>

## Abstract

The aim of this study was to reveal the mechanism of enhanced ram sperm motility induced by heavy ion radiation (HIR) after in vitro liquid storage. Ram semen was stored for 24 hours at 5°C and then irradiated with 0.1 Gy carbon ion radiation (CIR). In comparison to nonirradiated (NIR) sperm, the motility, viability, and adenosine triphosphate content were all higher in CIR sperm, and the reactive oxygen species levels were lower. Moreover, 87 differential mitochondrial protein spots were detected in 2-dimensional gels between CIR and NIR sperm and were identified as 52 corresponding proteins. In addition, 33 differential proteins were involved in a main pathway network, including COX5B, ERAB/HSD17B10, ETFA, SDHB, and SOD2, which are known to be involved in cell communication, energy production, and antioxidant responses. We used immunoblotting and immunofluorescence to analyze the content and localization of these proteins, respectively, and the levels of these proteins in CIR sperm were lower than those in NIR sperm. An understanding of the molecular function of these proteins could provide further insight into the mechanisms underlying high sperm motility induced by HIR in rams.

## Keywords

ram sperm, mitochondria, proteomics, carbon ion radiation

## Introduction

Since the sperm are quite resistant to radiation damage,<sup>1</sup> the use of radiation to improve the quality of mammalian sperm has been of increased concern to researchers in the recent years, previous studies have shown that X-rays can improve the sperm-fertilizing potential in cattle,<sup>2</sup> and the most representative study involves the use of laser radiation to improve rabbit and poultry sperm fertilization.<sup>3-5</sup> Although researchers have attempted to determine related biological effects and irradiation technology in mammalian sperm improvement, the research results have been inconclusive.

In the recent years, heavy ion radiation (HIR) has gradually entered the field of vision animal researchers because in vitro, HIR can improve the quality of human sperm,<sup>6</sup> which is of great significance for mammalian sperm improvement. In our previous studies, we determined the effects of carbon ion radiation (CIR) on ram sperm quality in vitro liquid. We also

confirmed that a suitable dose of CIR has a positive effect that can promote greater ram sperm motility and raise the adenosine triphosphate (ATP) content in sperm over 24 hours of in vitro

<sup>1</sup> College of Veterinary Medicine, Gansu Agricultural University, Lanzhou, China

<sup>2</sup> Department of Radiation Medicine, Institute of Modern Physics, Chinese Academy of Sciences, Lanzhou, China

<sup>3</sup> Key Laboratory of Radiation Biology and Medicine of Chinese Academy of Sciences, Lanzhou, China

<sup>4</sup> Key Laboratory of Basic Research on Heavy Ion Radiation Application in Medicine, Lanzhou, China

Received 11 May 2018; received revised 10 August 2018; accepted 29 August 2018

## Corresponding Author:

Xingxu Zhao, College of Veterinary Medicine, Gansu Agricultural University, Lanzhou 730070, China.

Email: zhaoux@gsau.edu.cn



Creative Commons Non Commercial CC BY-NC: This article is distributed under the terms of the Creative Commons Attribution-NonCommercial 4.0 License (<http://www.creativecommons.org/licenses/by-nc/4.0/>) which permits non-commercial use, reproduction and distribution of the work without further permission provided the original work is attributed as specified on the SAGE and Open Access pages (<https://us.sagepub.com/en-us/nam/open-access-at-sage>).

liquid storage at 15°C. Furthermore, we determined that the best suitable radiation dose for this purpose was 0.1 Gy.<sup>7</sup> There is, however, limited information available about the mechanism underlying enhanced sperm quality by HIR; thus, we need to delineate this potential mechanism.

He-Ne laser irradiation can increase mitochondrial electrochemical potential and increase ATP synthesis.<sup>8</sup> The ATP content was shown to be increased after HIR in our previous study,<sup>7</sup> which suggested to us that HIR improves sperm-fertilizing potential by changing sperm mitochondria function as a possible mechanism. Because mitochondria play a key role in energy production and maintenance of sperm motility,<sup>9</sup> this conclusion has encouraged us to believe that sperm mitochondria are the key reason that HIR can enhance ram sperm motility. Therefore, the aims of the present study were to examine the changes in the ram sperm mitochondrial proteome irradiated by HIR using a 2-dimensional gel electrophoresis (2-DE) approach to identify mitochondrial proteins that undergo abundant changes after HIR and to predict the biological functions and cellular pathways in the regulation of ram sperm motility after HIR.

## Materials and Methods

### Semen Collection, Dilution, and Examination

Using artificial vaginas, semen was collected 3 times (3 pools,  $n = 3$ ) from 5 mature and healthy Dorset rams (*Ovis aries*) under the same feeding conditions for 3 or 4 ejaculations/pool over 4 months. The pooled sperm concentration and motility were then assessed using a counting cell and an optical microscope (80i, Nikon, Tokyo, Japan) at 400 $\times$  magnification.<sup>10</sup> Only semen with a wave motion score >3 on a scale of 0 to 5, with a sperm concentration of >2.5  $\times 10^9$ /mL were accepted.<sup>11</sup> Each pool was mixed well and then further mixed with 5 $\times$  volume of diluent (2.422 g Tris, 1.34 g citric acid, 0.5 g fructose, 500 IU benzylpenicillin, and streptomycin in 100 mL deionized water).<sup>12,13</sup> The mixture was protected from light and incubated in water at 37°C in a vacuum cup for 30 minutes (volume 1.5 L; Wanxiang, China). All samples were then stored at 5°C for 24 hours.

### Irradiation

A heavy ion beam current,  $^{12}\text{C}^{6+}$  accelerated to 80 MeV/U and LET of 30 keV  $\mu\text{m}^{-1}$  at the beam entrance, was supplied by the Heavy Ion Research Facility in Lanzhou (HIRFL) at the Institute of Modern Physics, Chinese Academy of Sciences (Lanzhou, China). The dose rate was approximately 0.5 Gy  $\text{min}^{-1}$ , and the irradiated dose was 0.1 Gy. An air isolation room was used to detect the dose, and the acquisition of dose data was automatically controlled by a computer. Semen samples were divided into 2 parts after storage at 5°C for 24 hours. One part was not irradiated (the NIR group), whereas the other samples were irradiated with 0.1 Gy of the  $^{12}\text{C}^{6+}$  beam (the CIR group). The CIR group was irradiated at room temperature and first

placed in water at 37°C in a vacuum cup after irradiation and then immediately returned to the laboratory. The NIR group was kept the same temperature conditions with CIR group, and all experiments were performed within 30 minutes.<sup>7</sup>

### Sperm Motility and Viability

Sperm samples were diluted to 30  $\times 10^6$  sperm/mL with diluent, and sperm motility counts were determined using a counting cell chamber and light microscope at 400 $\times$  (Nikon 80i). Sperm motility (as a percentage) was calculated by dividing the number of motile sperm over the total number of sperm (both motile and nonmotile).<sup>14</sup>

Alexa Fluor<sup>®</sup> 488 Annexin V apoptosis kit (Thermo, Waltham, Massachusetts) was used to assess sperm viability. Briefly, 5  $\mu\text{L}$  of annexin V and 1  $\mu\text{L}$  of PI stock solution were added to the sperm suspension (100  $\mu\text{L}$ , 1  $\times 10^6$  sperm/mL) and incubated at room temperature for 15 minutes. The samples were then observed under a fluorescence microscope at a 400 $\times$  magnification (Nikon 80i). Viable sperm expressed the green fluorescence of Alexa Fluor 488 (excitation of 488 nm and emission of 530 nm) and nonviable sperm expressed the red fluorescence of PI (excitation of 535 nm and emission of 615 nm). At least 200 sperm were evaluated, and the percentage of viable sperm was calculated according to the following ratio: green cells/(green cells + red cells)  $\times 100\%$ .<sup>15</sup>

### Intracellular Reactive Oxygen Species and Determination of ATP Concentration

A sperm suspension (50  $\mu\text{L}$ ) was made in phosphate-buffered saline (PBS; 1  $\times 10^6$  sperm/mL) loaded with 5  $\mu\text{mol/L}$  2', 7'-dichlorofluorescein diacetate (DCFH-DA; Sigma Chemical, St Louis, Missouri). After incubation in the dark for 30 minutes, sperm were resuspended in 1 mL PBS. Cellular reactive oxygen species (ROS) were measured in 10 000 cells using a Varioskan Flash 3001 microplate reader (Thermo) at 470 nm excitation and 530 nm emission as a result of DCFH-DA oxidation.<sup>16</sup>

The ATP content was measured according to the protocol of the ATP assay kit (Beyotime, Shanghai, China). An aliquot of 1  $\times 10^6$  sperm was homogenized with 200  $\mu\text{L}$  of the lysis buffer supplied with the ATP assay kit and then vortexed for 1 to 2 seconds on a shaker. After centrifugation at 12 000  $\times g$  for 5 minutes at 4°C, the supernatant was transferred to a new tube for the ATP assay. Luminescence from a 100  $\mu\text{L}$  sample together with 100  $\mu\text{L}$  ATP detection buffer from the ATP assay kit was measured in a Varioskan Flash 3001 microplate reader (Thermo). The standard curve of ATP concentration was constructed from a known amount (1 nmol/L to 1 mol/L).<sup>17</sup>

### Measurement of Mitochondrial Membrane Potential

The mitochondrial membrane potential was assessed using an assay JC-1 kit (Beyotime). Briefly, approximately 2  $\times 10^7$  sperm were added into 500  $\mu\text{L}$  JC-1 stained working solution (1:200 dilution and final concentration 10 mg/mL) and

incubated at 37°C for 30 minutes. When the membrane potential is relatively low, JC-1 is capable of emitting green fluorescence. At a high membrane potential, JC-1 aggregates and produces red fluorescence. After incubation, samples were washed twice with the JC-1 wash buffer and suspended in the wash buffer before analysis. Fluorescence absorbance was measured using a Varioskan Flash 3001 microplate reader (Thermo). Activated mitochondria expressed red fluorescence of the JC-1 stain (J-aggregate, excitation of 525 nm and emission of 590 nm) and less activated mitochondria expressed green fluorescence of the JC-1 stain (J-monomer, excitation of 490 nm and emission of 530 nm). The mitochondrial membrane potential was calculated according to the following ratio: red fluorescence absorbance/green fluorescence absorbance.<sup>18</sup>

### **Transmission Electron Microscopy Observation of Mitochondrial Ultrastructure**

The sperm suspension (50  $\mu$ L) in PBS ( $1 \times 10^6$  sperm/mL) was centrifuged, and sperm were fixed with 2% glutaraldehyde, post-fixed with 1% osmium tetroxide, and embedded in resin. Ultrathin sections were cut and stained with uranyl acetate and lead citrate. Mitochondria are enriched in the midpiece of sperm, and the ultrastructure of the midpiece of ram sperm was determined using a transmission electron microscope (Hitachi H-7650; Hitachi Technologies, Tokyo, Japan).

### **Mitochondrial Extraction of Ram Sperm**

Mitochondria of ram sperm were isolated using a mitochondrial isolation kit (Beyotime). Semen samples were centrifuged at  $275 \times g$  for 10 minutes at room temperature to separate seminal plasma. The sperm pellet was resuspended in dilution buffer and centrifuged at  $800 \times g$  for 10 minutes at 4°C after which the supernatant was discarded. One mL of mitochondrial separation reagent was added per  $2 \times 10^6$  sperm to suspend the sperm pellet. The suspension was then homogenized on ice 30 times with a glass homogenizer and centrifuged at  $1000 \times g$  to remove other organelles. The supernatant was centrifuged at  $11\,000 \times g$  for 10 minutes at 4°C to collect the mitochondria. Purified mitochondria were frozen at  $-80^\circ\text{C}$  until proteomic analysis.

### **Two-Dimensional Electrophoresis, Image Analysis and Matrix-Assisted Laser Desorption/Ionization Tandem Time-of-Flight Mass Spectrometry Analysis**

Purified mitochondria were treated with a lysis buffer containing 7 mol/L urea, 2 mol/L thiourea, 4% (w/v) 3-[(3-cholamidopropyl)-dimethylammonio]-1-propane sulfonate (CHAPS), and 2% (w/v) dithiothreitol (DTT) in the presence of 1% (V/W) protease inhibitor cocktail (Sigma Chemical, St Louis, Missouri). Protein concentration was measured by the Bio-Rad Bradford protein assay using bovine serum albumin (Sigma) as a standard.

Each 300  $\mu$ g mitochondrial protein sample was dissolved in 350  $\mu$ L of rehydration buffer and loaded into a 17-cm immobilized pH gradient (IPG) strip (Bio-Rad Laboratories, Hercules, California) at pH 3 to 10, after which separation was conducted using the IPGphor isoelectric focusing system (IEF). The program settings were as follows: 14 hours at 50 V; 1 hour at 250 V; 1000 V for 1 hour; 9000 V for 6 hours; and 9000 V for 8 hours.<sup>19,20</sup> Following isoelectric focusing, the focused IPG strips were equilibrated in buffer containing 6.0 mol/L urea, 375 mmol/L Tris, 20% glycerol, 2% sodium lauryl sulfate, and 130 mmol/L DTT for 10 minutes in buffer containing 350 mmol/L acrylamide monomer. Alkylation in the buffer occurred for 10 minutes. The second dimension was carried out on a large polyacrylamide gel ( $18 \times 18 \times 0.1$  cm) with a 12% stacked gel. The focused IPG strips were sealed to the top of the stacked gel with a 0.5% low melting agarose solution in 375 mmol/L Tris and 0.007% bromophenol blue. Electrophoresis was performed at 4°C and the gel was run in a Protean II xi Cell (Bio-Rad) at a constant current of 24 mA/gel for  $\sim 8$  hours with a maximum limit of 300 V.<sup>21,22</sup> Upon completion, the gel was stained with silver nitrate and destained with ultrapure water.<sup>23</sup> Three 2-DE gels were prepared for each sample, scanned with an Epson scanner, and stored as TIF files. The PDQuest 8.0 software (Bio-Rad) was used to detect and match spots. Spots were selected if the difference in protein quantity was  $\geq 2$ -fold (normalized spot volume) between control and irradiated groups. The mass spectrometry (MS) and MS/MS data for protein identification were obtained using a matrix-assisted laser desorption/ionization tandem time-of-flight mass spectrometry instrument (4800 Proteomics Analyzer; Applied Biosystems). Instrument parameters were set using the 4000 Series Explorer software (Applied Biosystems).

### **Immunoblotting and Immunofluorescence**

The 5 commercial primary antibodies used were rabbit polyclonal IgG anti-COX5B (Cat. #bs-3931R); mouse polyclonal IgG anti-ERAB/HSD17B10 (Cat. #bs-0021M); rabbit polyclonal IgG anti-ETFA (Cat. #bs-0494R); rabbit polyclonal IgG anti-SDHB (Cat. #bs-6650R); rabbit polyclonal IgG anti-SOD2 (Cat. #bs-20667R; Bioss Biotechnology Co, Ltd, Beijing, China), and rabbit polyclonal IgG anti- $\beta$ -actin (Cat. #AP0060; Bioworld technology, Inc, Ltd, Nanjing, China). A 30  $\mu$ g of sperm protein was separated by sodium dodecyl sulfate polyacrylamide gel electrophoresis and transferred to a polyvinylidene fluoride membrane. The membrane was blocked with 5% skimmed milk in Tris-buffered saline (TBS) and immunoblotted with primary antibody and horseradish peroxidase (HRP)-labeled secondary antibody (ZDR-5308; Zhongshan Jinqiao Biotechnology Co., Ltd., Beijing, China). Immunoreactivity was detected using an enhanced chemiluminescent HRP substrate kit (BLH01S050; Bioworld), and images were captured by a FluorChem 2 imaging system (Alpha Innotech, San Leandro, California). The Quantity One 4.5.2 image analysis software (Bio-Rad) was used to quantitatively analyze the relative density of bands in Western blots.

**Table 1.** Comparison of Motility, Viability, Mitochondrial Function, and ATP and ROS Contents in Ram Sperm Subjected to CIR after 24 h of In Vitro Liquid Storage at 5°C.<sup>a,b</sup>

	NIR	CIR
Motility, %	57.67 ± 0.0206	62.37 ± 0.0344 <sup>c</sup>
Viability, %	64.92 ± 6.073	66.04 ± 5.11
JC-1	1.127 ± 0.0897	1.48 ± 0.0625 <sup>c</sup>
ATP, mmol/μg	1.915 ± 0.157	2.335 ± 0.2436 <sup>c</sup>
ROS (DCF absorbance)	22.25 ± 1.5	19 ± 0.8165 <sup>d</sup>

Abbreviations: CIR, Ram Sperm Subjected to 0.1 Gy Carbon ion Radiation; NIR, Non-Irradiated Ram Sperm.

<sup>a</sup>Values Represent Mean ± SEM (n = 3).

<sup>b</sup>Asterisks denote values that are significantly different from those of NIR sperm

<sup>c</sup>P < .01 with Student t test analysis.

<sup>d</sup>P < .05 with Student t test analysis.

The data were corrected for the background and expressed as the optical density (OD/mm<sup>2</sup>).

Sperm samples were suspended in PBS and then air-dried on microscope slides at room temperature and fixed in methanol. The slides were then washed 3 times in PBS for 10 minutes and blocked for 1 hour at room temperature in 5% bovine serum albumin (BSA). Slides were incubated for 1 hour with the primary antibodies (1:500) and then washed 3 times in PBS. The sperm were incubated in the secondary antibodies Alexa Fluor 555 (rabbit IgG, bs-0295P-A555; 1:100) and Alexa Fluor 555 (Mouse IgG, bs-0296P-A555; 1:100; Bioss), for 1 hour at room temperature. Slides were then washed and counterstained with 4,6-diamidino-2-phenylindole before being placed on a coverslip. Negative controls were obtained using similar techniques but with the omission of the primary antibody. Images were obtained using a confocal laser microscope (LSM, Oberkochen, Germany) and camera. Sperm exhibiting red fluorescence were considered positive.<sup>24</sup>

### Statistical Analysis

Data are presented as mean ± standard error of mean (SEM). Student *t* test was used to analyze differences in the SPSS/PC program (Version 19.0; SPSS Inc, Chicago, Illinois). *P* < .05 was considered statistically significant.

## Results

### Analysis of Sperm Motility and Viability

To investigate the effects of CIR on ram sperm after 24 hours of storage at 5°C, sperm motility and viability were examined. Greater motility was observed in the CIR group (Table. 1; *P* < .01); however, there were no changes in sperm apoptosis in the CIR group using Alexa Flour 488 annexin V/PI staining (Table. 1). These results indicate that 0.1 Gy CIR treatment after 24 hours of storage at 5°C can improve ram sperm motility, and imposes no harm on sperm viability compared to NIR sperm.

### Analysis of ATP Content

The ATP has a direct effect on sperm motility. Therefore, the ATP content was measured to determine whether or not HIR improves ram sperm motility through an increase in ATP content; 0.1 Gy CIR treatment significantly increased ATP content in ram sperm (Table. 1; *P* < .01). These results suggest that CIR improves ram sperm motility after 24 hours of storage at 5°C by increasing ATP content.

### Analysis of ROS Content

In vitro liquid storage of sperm for over 24 hours was implemented to increase the formation of ROS in sperm and then disrupt the antioxidative system in sperm and decrease sperm motility. Therefore, ROS content was measured to determine whether or not CIR improves ram sperm motility by decreasing ROS content. A significant decrease in ROS content was observed in ram sperm following CIR treatment with 0.1 Gy (Table. 1; *P* < .05). These results suggest that CIR can decrease ROS content in ram sperm after 24 hours of storage at 5°C.

### Analysis of Ultrastructure of Midpiece in Ram Sperm

Mitochondria are mainly involved in the formation of the midpiece of sperm; therefore, transmission electron microscopy was used to evaluate any damage to the ultrastructure of the midpiece in ram sperm (Figure. 1). No obvious damage nor notable differences in the ultrastructure of the mitochondria were noted in the NIR and CIR ram sperm. Sperm exhibited tightly arranged, intact mitochondria around the axons. This indicated that 0.1 Gy CIR treatment did not harm the ultrastructure of the midpiece nor the mitochondrial arrangement in ram sperm after 24 hours of storage at 5°C.

### Analysis of Mitochondrial Function

Mitochondria are the energy centers of sperm and they directly affect sperm motility and energy supply. Following JC-1 staining, which was used to evaluate mitochondrial function, a significant increase in the proportion of red/green fluorescence absorbance was observed in the group treated with 0.1 Gy CIR (Table 1; *P* < .01). These data indicated that CIR treatment improved mitochondrial function in ram sperm after 24 hours of storage at 5°C.

### Identification of Differential Mitochondrial Proteins

We performed 2-DE experiments to investigate the differential mitochondrial proteins in NIR and CIR sperm, and the protein profiles are shown in Figure. 2. PDQuest 8.0 software was used to detect differential protein spots, and ≥2-fold difference in the protein quantities (normalized spot volume) was used as the standard to detect differential protein spots. Based on analysis of the 2-D gels, a significant proteome difference between the NIR and the CIR sperm was observed, and 87 differential protein spots were detected. Among the 87 protein spots that were evident, the volume of 19 spots was increased and that of 68 spots was reduced in the CIR group (Figure. 2). A list of

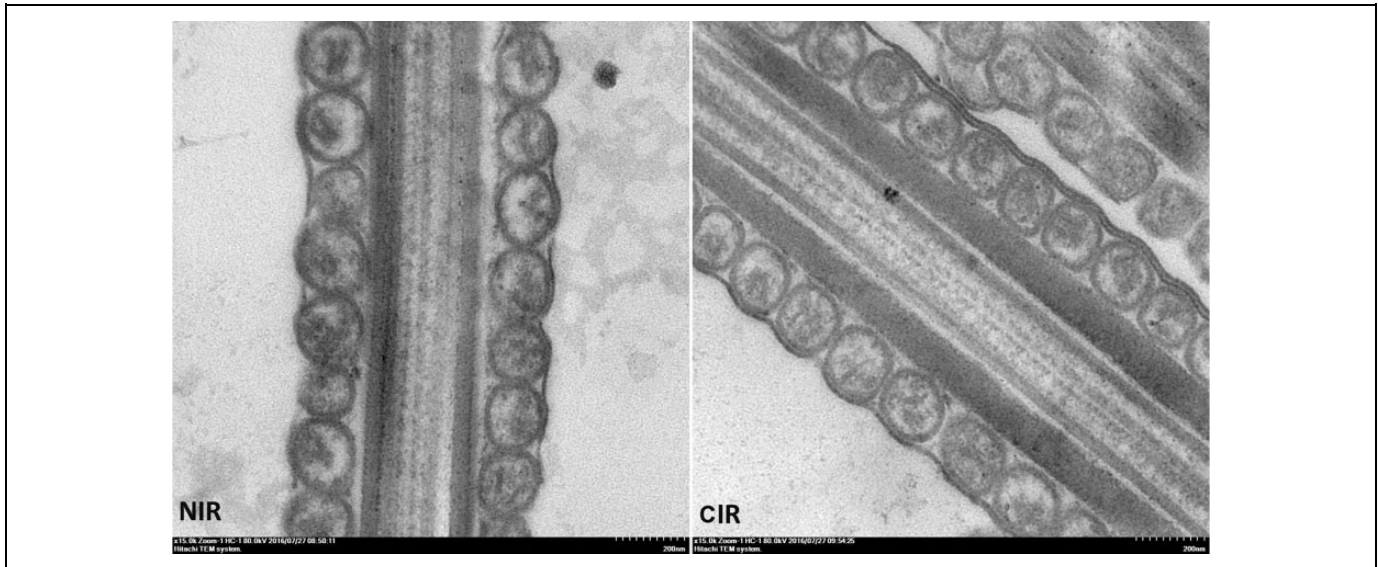


**Figure 1.** Mitochondria are mainly involved in the formation of the midpiece of sperm. The representative ultrastructure of the midpiece in ram sperm was observed using transmission electron microscopy. NIR indicates non-irradiated ram sperm; CIR, ram sperm subjected to 0.1 Gy carbon ion radiation.

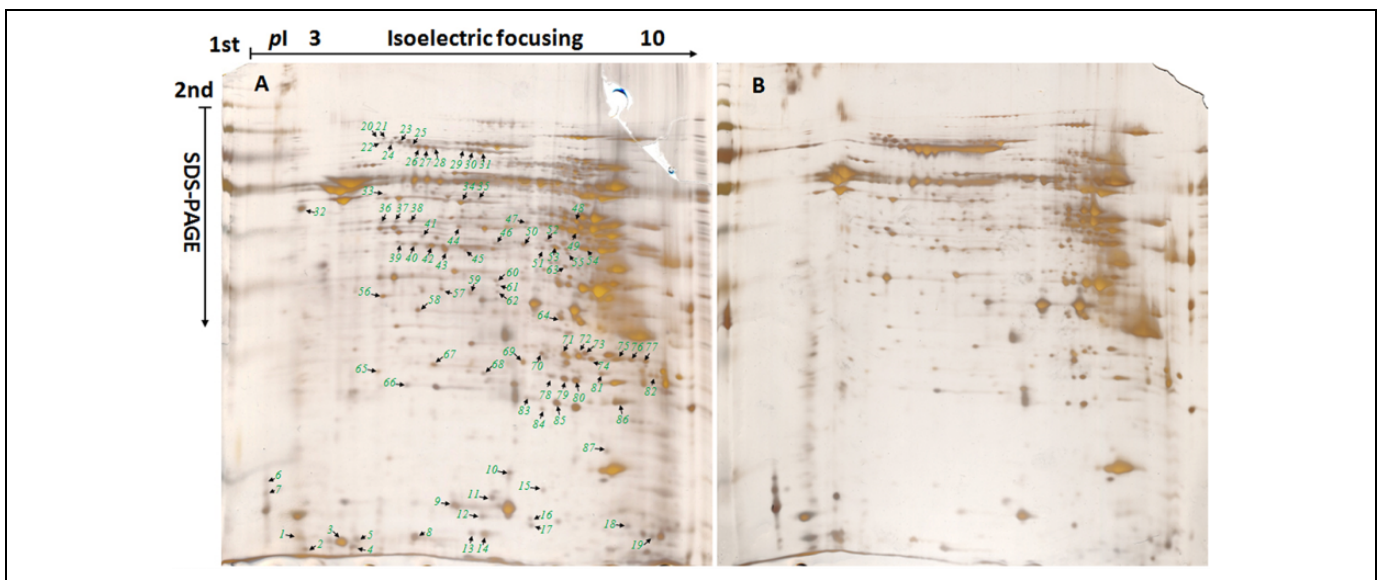


**Figure 2.** Protein profiles and differential protein spots of ram sperm subjected to carbon ion radiation after 24 hours of in vitro liquid storage at 5°C. Proteins (300 µg) were separated using an isoelectric focusing system (IEF) at pH 3 to 10, followed by 12% SDS-PAGE, and subsequently visualized by silver staining. A, Nonirradiated ram sperm. B, Ram sperm subjected to 0.1 Gy carbon ion radiation. Green arrows represent differential protein spots. Spot numbers of representative proteins are in accordance with Table 2.

differential proteins and their potential function is shown in Table 2. These 87 protein spots were identified as 52 proteins. The fold-change of the proteins (ratio of CIR-to-NIR) was converted to generate a heatmap representing differential proteins using R/Bioconductor software (Figure 3A).

### *Bioinformatic Analysis of the Differential Mitochondrial Proteins*

The differential mitochondrial proteins of ram sperm were grouped using Gene Ontology (GO) annotation and classified

by biological process, cellular function, and molecular function. Using the biological process database, the metabolic process (15%) was associated with energy production (Figure 3Ba). The remaining proteins were involved in organelle, cell, extracellular region, membrane-enclosed lumen, cell junction, and macromolecular complex (Figure 3Bb). An analysis of molecular function demonstrated that the majority of the proteins were classified as proteins with catalytic and binding features (Figure 3Bc). The Kyoto Encyclopedia of Genes and Genomes (KEGG) enrichment showed the differential mitochondrial proteins can be enriched in 10 biological process

**Table 2.** Differential Mitochondrial Proteins in Ram Sperm Subjected to Carbon ion Radiation After 24 Hours of In Vitro Liquid Storage at 5°C.

Protein Spot	Protein Name	Abbreviation	Accession (NCBI)	pI/Mw	Peptide Count	Protein Score	Cover (%) <sup>a</sup>	Average Fold Change <sup>b</sup>
Spot 2	A-kinase anchor protein 3 isoform X2 [Ovis aries]	Akap3	gi 426225692	6.72/94987.2	20	252	23.03%	0.227 ± 0.011
Spot 3	Cytochrome C oxidase subunit 5A, mitochondrial isoform X1 [Ovis aries]	Cox5a	gi 803178620	6.42/16925.7	9	312	40.13%	0.17 ± 0.015
Spot 4	Glutathione transferase M3, partial [Ovis aries]	Gstm3	gi 78557758	5.91/15606.6	1	147	60%	0.33 ± 0.057
Spot 5	Ropporin-1A [Ovis aries]	Ropn1	gi 803241098	5.3/24070.4	4	213	25.94%	0.4 ± 0.01
Spot 6	Calmodulin isoform X2 [Ovis aries]	Calm1	gi 803262026	4.09/16826.8	4	130	24.16%	0.036 ± 0.02
Spot 7	Calmodulin-alpha [Ovis aries]	Calma	gi 803055820	4.04/16384.6	5	132	36.55%	0.4 ± 0.07
Spot 8	Glutathione transferase M3, partial [Ovis aries]	Gstm3	gi 78557758	5.91/15606.6	15	493	87.69%	0.433 ± 0.047
Spot 9	Peroxiredoxin-5, mitochondrial [Ovis aries]	Prdx5	gi 426251990	8.62/23434.3	10	222	44.29%	0.12 ± 0.009
Spot 10	Peroxiredoxin-5 [Ovis aries]	Prdx5	gi 429999293	6.3/17477.2	8	146	59.88%	0
Spot 11	A-kinase anchor protein 3 isoform X2 [Ovis aries]	Akap3	gi 803249561	6.72/94969.2	18	179	20.92%	0.417 ± 0.028
Spot 12	Histidine triad nucleotide-binding protein 2, mitochondrial isoform X2 [Ovis aries]	Hint2	gi 426220220	9.03/17276.3	10	521	68.71%	0.166 ± 0.057
Spot 14	Cytochrome c oxidase subunit 5B, mitochondrial [Ovis aries]	Cox5b	gi 803291371	8.8/13979.1	6	128	46.51%	0.326 ± 0.068
Spot 16	Histidine triad nucleotide-binding protein 2, mitochondrial isoform X2 [Ovis aries]	Hint2	gi 426220220	9.03/17276.3	8	300	75.97%	0
Spot 17	Histidine triad nucleotide-binding protein2, mitochondrial isoform X2 [Ovis aries]	Hint2	gi 426220220	9.03/17276.3	5	99	42.31%	0
Spot 18	Cytochrome c oxidase subunit 4 isoform 1, mitochondrial isoform X2 [Ovis aries]	Cox4i1	gi 803258191	9.32/19602.1	8	134	36.69%	0.083 ± 0.07
Spot 20	NADH-ubiquinone oxidoreductase 75 kDa subunit, mitochondrial [Ovis aries]	Ndufs1	gi 426221412	5.9/80460.8	19	113	22.42%	0.123 ± 0.005
Spot 22	Keratin, type II cytoskeletal 3 isoform X1 [Ovis aries]	Krt2	gi 803057648	8.54/62318	18	70	30.59%	0.456 ± 0.051
Spot 25	Full = Actin, cytoplasmic I; AltName: Full = Beta-actin; Contains: RecName: Full = Actin, cytoplasmic I, N-terminally processed	Actb	gi 46397336	5.29/42051.9	10	132	41.07%	6.746 ± 0.566
Spot 26	Outer dense fiber protein 2 isoform X9 [Ovis aries]	Odf2	gi 426222964	7.52/76248.9	27	103	26.48%	20.82 ± 5.81
Spot 27	Outer dense fiber protein 2 isoform X11 [Ovis aries]	Odf2	gi 803031831	5.86/69017.4	22	72	30.22%	13.37 ± 1.862
Spot 28	Outer dense fiber protein 2 isoform X11 [Ovis aries]	Odf2	gi 803031831	5.86/69017.4	27	166	30.56%	4.796 ± 0.697
Spot 29	Succinate dehydrogenase [ubiquinone] flavoprotein subunit, mitochondrial isoform X2 [Ovis aries]	Sdha	gi 803240872	6.89/73997.6	30	334	27.52%	5.64 ± 1.25
Spot 30	Succinate dehydrogenase [ubiquinone] flavoprotein subunit, mitochondrial isoform X2 [Ovis aries]	Sdha	gi 803240872	6.89/73997.6	28	370	25.86%	99.33 ± 4.48
Spot 31	Succinate dehydrogenase [ubiquinone] flavoprotein subunit, mitochondrial isoform X2 [Ovis aries]	Sdha	gi 803240872	6.89/73997.6	32	960	25.41%	88.6 ± 6.63
Spot 34	Tektin-2 [Ovis aries]	Tekt2	gi 802976927	5.87/50359.9	27	649	39.53%	0.146 ± 0.005
Spot 35	Tektin-1 [Ovis aries]	Tekt1	gi 426237356	5.83/48956.5	21	107	39.23%	0

(continued)

**Table 2.** (continued)

Protein Spot	Protein Name	Abbreviation	Accession (NCBI)	pI/Mw	Peptide Count	Protein Score	Cover (%) <sup>a</sup>	Average Fold Change <sup>b</sup>
Spot 36	Succinyl-CoA ligase [GDP-forming] subunit beta, mitochondrial isoform XI [Ovis aries]	Suclg2	gi 426249303	6.78/46950.8	12	83	28.94%	0.126 ± 0.0047
Spot 37	Succinyl-CoA ligase [ADP-forming] subunit beta, mitochondrial [Ovis aries]	Sucla2	gi 426236317	6.48/50501.4	10	85	17.49%	0.3733 ± 0.034
Spot 38	Succinyl-CoA ligase [ADP-forming] subunit beta, mitochondrial [Ovis aries]	Sucla2	gi 426236317	6.48/50501.4	15	172	26.13%	0.126 ± 0.005
Spot 39	Succinyl-CoA:3-ketoacid coenzyme A transferase 2, mitochondrial isoform XI, partial [Ovis aries]	Oxct1	gi 803006295	7.25/54416.1	9	191	23.03%	0.033 ± 0.023
Spot 40	Succinyl-CoA:3-ketoacid coenzyme A transferase 2, mitochondrial isoform XI, partial [Ovis aries]	Oxct1	gi 803006295	7.25/54416.1	10	122	22.42%	0.23 ± .01
Spot 41	Nucleoside diphosphate kinase 7 isoform XI [Ovis aries]	Nme7	gi 803127740	5.66/45078.6	6	90	17.97%	0.3733 ± 0.0838
Spot 42	Succinyl-CoA:3-ketoacid coenzyme A transferase 2, mitochondrial isoform XI, partial [Ovis aries]	Oxctb	gi 803006295	7.25/54416.1	15	383	35.56%	0.346 ± 0.102
Spot 43	Isocitrate dehydrogenase [NAD] subunit alpha, mitochondrial isoform XI [Ovis aries]	ldh3a	gi 803178490	6.76/40128.3	20	245	39.34%	0.366 ± 0.017
Spot 44	Medium-chain specific acyl-CoA dehydrogenase, mitochondrial-like, partial [Ovis aries musimon]	Acadm	gi 803341491	8.09/15331.9	3	102	28.26%	0.23 ± 0.01
Spot 45	Isocitrate dehydrogenase [NAD] subunit alpha, mitochondrial isoform XI [Ovis aries]	ldh3a	gi 803178490	6.76/40128.3	12	145	25.68%	0.230 ± 0.075
Spot 46	Short-chain specific acyl-CoA dehydrogenase, mitochondrial isoform X2 [Ovis aries musimon]	Acads	gi 803214829	8.41/44870.9	12	95	30.83%	0
Spot 47	Ecotropic viral integration site 5 protein homolog isoform X2 [Ovis aries musimon]	Evi5	gi 803313859	5.89/101718.5	27	75	20.20%	0.173 ± 0.035
Spot 48	Fumarate hydratase [Ovis aries]	Fh	gi 238799808	8.97/54758.3	19	673	30.39%	0.353 ± .077
Spot 49	Citrate synthase, mitochondrial [Ovis aries]	Cs	gi 426224953	8.12/52026.6	22	611	31.55%	0.17 ± 0.01
Spot 50	Short-chain specific acyl-CoA dehydrogenase, mitochondrial isoform X2 [Ovis aries musimon]	Acads	gi 803214829	8.41/44870.9	19	342	39.81%	0.213 ± 0.06
Spot 54	Enoyl-CoA delta isomerase 2, mitochondrial isoform XI [Ovis aries]	Eci2	gi 803189412	8.39/38147.3	19	420	39.83%	0.05 ± 0.026
Spot 56	Radial spoke head protein 9 homolog isoform XI [Ovis aries]	Rsph9	gi 426250347	5.4/31373.2	17	164	62.32%	0.37 ± 0.173
Spot 57	Fumarylacetoacetate hydrolase domain-containing protein 2A [Ovis aries musimon]	Fahd2	gi 803291512	6.46/34937.2	10	116	27.71%	0.153 ± 0.025
Spot 59	Triosephosphate isomerase isoform X2 [Ovis aries musimon]	Tpi1	gi 803249757	6.14/30952.8	15	286	56.64%	0.178 ± 0.398
Spot 60	3-mercaptopyruvate sulfurtransferase isoform X2 [Ovis aries musimon]	Mpst	gi 803289122	6.16/33416.9	15	333	46.13%	0.083 ± .032
Spot 63	Alcohol dehydrogenase [NADP(+)] isoform XI [Ovis aries musimon]	Akr1a1	gi 803254329	8.14/40182.8	16	359	39.27%	0.086 ± 0.425
Spot 64	Electron transfer flavoprotein subunit alpha, mitochondrial isoform X2 [Ovis aries musimon]	Etfa	gi 803261858	8.77/35341.7	16	231	50.15%	0.243 ± 0.011
Spot 65	Keratin, type I cytoskeletal 14 isoform XI [Ovis aries]	Krt14	gi 803121007	5.18/49277.1	19	117	54.67%	0.296 ± 0.056

(continued)

**Table 2.** (continued)

Protein Spot	Protein Name	Abbreviation	Accession (NCBI)	pI/Mw	Peptide Count	Protein Score	Cover (%) <sup>a</sup>	Average Fold Change <sup>b</sup>
Spot 71	Mycophenolic acid acyl-glucuronide esterase, mitochondrial [Ovis aries]	Abhd10	gi 426217433	8.93/34456	12	184	32.03%	0.38 ± 0.017
Spot 72	Mycophenolic acid acyl-glucuronide esterase, mitochondrial [Ovis aries]	Abhd10	gi 426217433	8.93/34456	10	140	25.49%	0.07 ± 0.026
Spot 73	Keratin, type I cytoskeletal 10 isoform X3 [Ovis aries musimon]	Krt10	gi 803275000	5.05/56622.9	14	296	27.79%	0.4 ± 0.01
Spot 74	Enoyl-CoA hydratase, mitochondrial isoform X2 [Ovis aries musimon]	Echs1	gi 803206513	8.76/31564.3	8	248	34.14%	0.336 ± 0.068
Spot 75	Succinate dehydrogenase [ubiquinone] iron-sulfur subunit, mitochondrial isoform X6 [Ovis aries musimon]	Sdhb	gi 803326996	8.98/32324	20	424	40%	0.38 ± 0.017
Spot 76	GTP: AMP phosphotransferase AK3, mitochondrial isoform X1 [Ovis aries]	Ak3	gi 426220398	9.02/25682.5	14	415	60.35%	0.07 ± 0.026
Spot 77	GTP: AMP phosphotransferase AK3, mitochondrial isoform X1 [Ovis aries]	Ak3	gi 426220398	9.02/25682.5	18	426	60.79%	0.04 ± 0.01
Spot 78	Full = Actin, cytoplasmic I; AltName: Full = Beta-actin; Contains: RecName: Full = Actin, cytoplasmic I, N-terminally processed	Actb	gi 46397336	5.29/42051.9	11	117	42.13%	0.338 ± 0.068
Spot 79	Chromosome 21 open reading frame 33 [Ovis aries]	C21orf33	gi 238799774	8.76/28898.1	11	296	35.77%	0.227 ± 0.0323
Spot 80	Chromosome 21 open reading frame 33 [Ovis aries]	C21orf33	gi 238799774	8.76/28898.1	15	406	48.18%	0.35 ± 0.6245
Spot 81	3-hydroxyacyl-CoA dehydrogenase type-2 [Ovis aries]	Hsd17b10	gi 426256978	8.45/27323.3	9	280	41%	0.317 ± 0.052
Spot 82	Protein NipSnap homolog 3A isoform X1, partial [Ovis aries]	Nlpsnap3a	gi 803029850	9.07/27383.1	5	110	20.94%	0.24 ± 0.017
Spot 83	Mitochondrial superoxide dismutase 2 [Ovis aries]	Sod2	gi 256665379	8.89/24735.7	7	77	28.83%	0.196 ± 0.058
Spot 84	ATP synthase subunits, mitochondrial isoform X1 [Ovis aries]	Atp5s	gi 426233112	8.11/23659	13	165	54.50%	0.133 ± 0.015
Spot 85	Mitochondrial superoxide dismutase 2 [Ovis aries]	Sod2	gi 256665379	8.89/24735.7	7	362	22.52%	0.243 ± 0.115
Spot 86	Keratin, type II cytoskeletal I isoform X1 [Ovis aries]	Krt1	gi 803043128	7.62/62447.5	18	102	27.67%	0.35 ± 0.06

Abbreviations: pI, Isoelectric Point; Mw, Molecular Weight; NCBI, National Center of Biotechnology Information.

<sup>a</sup>Peptides matched refers to the matched peptides to the amino acids of the full-length protein.

<sup>b</sup>Match between non-irradiated sperm and sperm subjected to carbon ion radiation (gels of  $3 \times 0.1$  Gy carbon ion radiation vs nonirradiated sperm;  $n = 3$  in each group).

(Figure 3C). The protein–protein interaction network was analyzed using a publicly available program (<http://www.omicsbean.com>), and the interaction network included 33 proteins involved in 10 biological process (Figure 3D).

### Immunoblotting and Immunofluorescence Analysis of 5 Different Proteins

Immunoblotting and immunofluorescence analysis using the abovementioned commercial primary antibodies resulted in the detection of the 5 proteins in NIR and CIR sperm (Figures 4 and 5). Compared to NIR sperm, the content of these 5 proteins was significant decreased in CIR sperm (Figure 4B;  $P < .01$ ,  $P < .001$ ). The localization of these 5 proteins in sperm was also

analyzed, and the fluorescence was distributed on acrosome and midpiece of sperm (Figure 5A–J). None of the 5 candidate proteins was detected in the sperm tail. The fluorescence strength of the 5 proteins was weak in CIR ram sperm. The immunoblotting and immunofluorescence results were consistent with those of the 2-DE analyses.

### Discussion

We have demonstrated that HIR treatment can improve ram sperm motility after 24 hours of in vitro liquid storage<sup>7</sup>; however, the mechanism underlying this phenomenon remains unclear. In the present study, we focused on the mitochondrial function combined with 2-DE to reveal the underlying



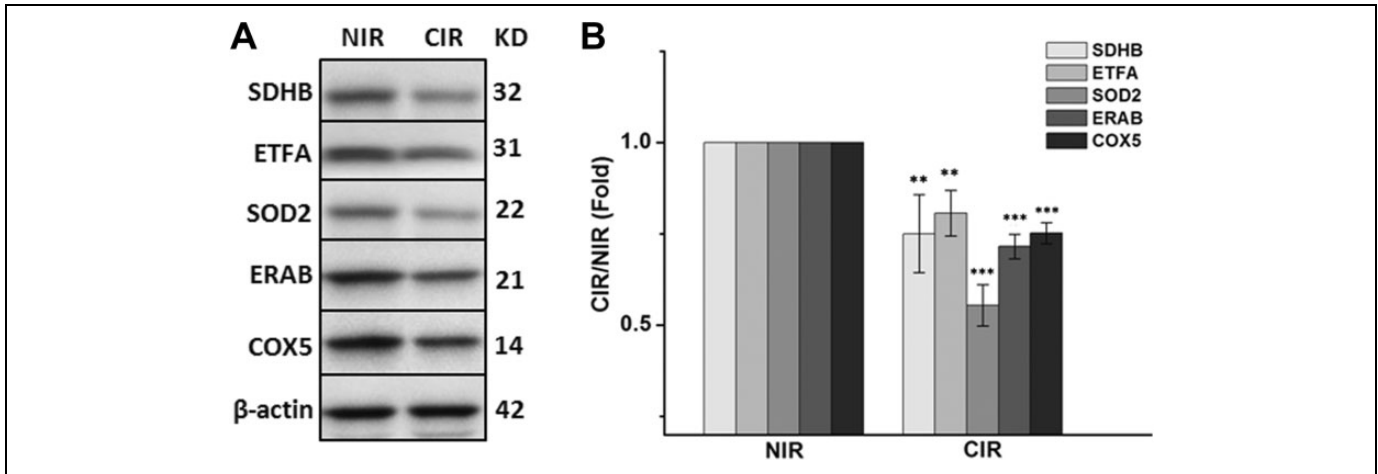


**Figure 4.** A, Representative immunoblotting of 5 proteins in ram sperm. B, Relative protein content; values represent the mean  $\pm$  SEM from 3 gels per group; asterisks indicate a statistically significant difference from NIR sperm; \*\* $P < .01$  and \*\*\* $P < .001$  with Student *t* test analysis. NIR indicates nonirradiated ram sperm; CIR, ram sperm subjected to 0.1 Gy carbon ion radiation.

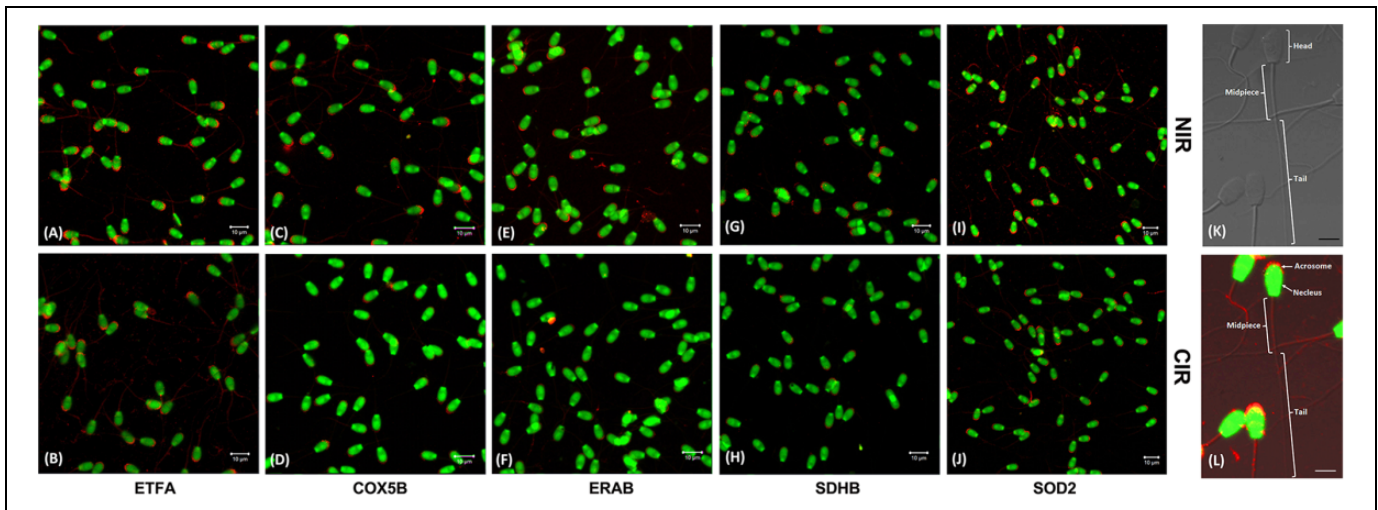


**Figure 5.** Immunofluorescence localization analysis of 5 proteins in ram sperm subjected to carbon ion radiation after 24 hours of in vitro liquid storage at 5°C. (A–J), magnification  $\times 400$ ; K and L, magnification  $\times 1000$ ; scale bar = 10  $\mu$ m; DAPI (nucleus, green) and target protein (red). A, C, E, G, and I indicate NIR sperm; B, D, F, H, and J indicate CIR sperm; K and L indicate the morphological characteristics of different parts of the ram sperm; K was observed under a differential interference contrast microscope (DIC); L represents the merging of DIC and immunofluorescent images (red, ETF A). NIR, non-irradiated ram sperm; CIR, ram sperm subjected to 0.1 Gy carbon ion radiation.

mechanism that HIR treatment can improve ram sperm motility after storage at 5°C for 24 hours. Improvements in sperm quality following HIR involve use of new techniques for maintaining highly motile sperm. Therefore, with ram sperm motility, the role of HIR in improving sperm quality has important practical significance. Such improvement can contribute effectively in the enhancement of artificial insemination conditions.

#### *HIR Treatment can Improve Mitochondrial Function and Anti-Oxidative Ability to Increase Ram Sperm Motility After Storage for 24 hours at 5°C*

In the present study, we demonstrated that 0.1 Gy CIR treatment affected the metabolic pathways related to energy

production in ram sperm after storage for 24 hours. These results indicated that HIR treatment might mediate mitochondrial oxidative phosphorylation (OXPHOS) and other metabolic pathways to produce more energy for ram sperm motility. Because OXPHOS is the main energy source under normal conditions, under pathologic conditions, OXPHOS was blocked. Thus, sperm could activate other metabolic pathways, such as glycolysis, the TCA cycle, and fatty acid degradation to maintain the energy supply for sperm motility.<sup>25</sup> Therefore, we speculate that ram sperm stored at 5°C for 24 hours could have an impact on OXPHOS and was gradually weakened, while other metabolic pathways were gradually increased to maintain ATP balance. The ATP content was correspondingly reduced because the efficiency of ATP of other metabolic pathways was



humans, dogs, and other species.<sup>44</sup> TPI1 catalyzes the conversion of dihydroxyacetone phosphate to glyceraldehyde-3-phosphate, and glyceraldehyde-3-phosphate dehydrogenase catalyzes glyceraldehyde-3-phosphate to glycerol 1,3-bisphosphate and then produces ATP in the following steps.<sup>45</sup> The relationship between TPI1 level and frozen–thawed boar sperm has been demonstrated. The frozen–thawed process can decrease the boar sperm motility; however, the levels of TPI1 are increased in frozen–thawed boar sperm.<sup>45</sup> In this study, the relationship between decreased Tekt1 and TPI1, and ram sperm motility should be further confirmed.

In this study, the level of 5 proteins (COX5B, ERAB/HSD17B10, ETFA, SDHB, and SOD2) was verified using immunoblotting and immunofluorescence. The results showed differences in the levels of these 5 proteins between the NIR and CIR groups, and their levels were decreased in the CIR group and were consistent with the 2-DE results, which indicates that these 5 proteins could play a potential role in improving mitochondrial function of ram sperm induced by CIR after in vitro liquid storage.

## Conclusions

This is the first comprehensive description of mitochondria in ram sperm to reveal the underlying mechanism that 0.1 Gy CIR treatment can improve ram sperm motility after in vitro liquid storage for 24 hours at 5°C. The present study has identified differential proteins and the pathways relevant to sperm motility and those that could likely be altered in ram sperm resulting in the manifestation high motility after 0.1 Gy CIR. These mitochondrial proteins that undergo abundant changes after 0.1 Gy CIR and predict the biological functions and cellular pathways in the regulation of ram sperm motility after CIR.

## Declaration of Conflicting Interests

The author(s) declared no potential conflicts of interest with respect to the research, authorship, and/or publication of this article.

## Funding

The author(s) disclosed receipt of the following financial support for the research, authorship, and/or publication of this article: This research was supported by the Scientific Research Start-up Funds for Openly-Recruited Doctors of Gansu Agricultural University (2017RCZX-13), the National Natural Science Foundation of China (11505244, 11875061), the Western Talent Program of the Chinese Academy of Sciences (Y560020XB0), the Special Funds for Discipline Construction of Gansu Agricultural University (GAU-XKJS-2018-067), the National High Technology Research and Development Program of China (2013AA102505), and the Ministry of Science and Technology National Key R&D project (2016YFC0904600).

## References

1. Van Herpen G, Rikmenspoel R. Radiation damage to bull sperm motility. I. X-ray effects and target theory. *Biophys J.* 1969;9(6): 822-832.
2. Rikmenspoel R. Radiation damage to bull sperm motility. III. Further X-ray studies. *Biophys J.* 1975;15(8):831-841.
3. Iaffaldano N, Meluzzi A, Manchisi A, Passarella S. Improvement of stored turkey semen quality as a result of He–Ne laser irradiation. *Anim Reprod Sci.* 2005;85(3-4):317-325.
4. Iaffaldano N, Rosato MP, Paventi G, et al. The irradiation of rabbit sperm cells with He–Ne laser prevents their in vitro liquid storage dependent damage. *Anim Reprod Sci.* 2010;119(1-2): 123-129.
5. Iaffaldano N, Paventi G, Pizzuto R, et al. The post-thaw irradiation of avian spermatozoa with He–Ne laser differently affects chicken, pheasant and turkey sperm quality. *Anim Reprod Sci.* 2013;142(3-4):168-172.
6. Zhang H, Wei ZQ, Li WJ, et al. Effects of 16O+6 ion irradiation on human sperm spontaneous chemiluminescence, motility, acrosome reaction and viability in vitro. *Shi Yan Sheng Wu Xue Bao.* 1999;32(1):1-6.
7. He Y, Li H, He J, Zhao X. Heavy ion radiation can promote greater motility and enolase protein expression in ram sperm in *in vitro* liquid storage. *Anim Reprod Sci.* 2014;148(3-4):260-266.
8. Passarella S, Casamassima E, Molinari S, et al. Increase of proton electrochemical potential and ATP synthesis in rat liver mitochondria irradiated in vitro by helium–neon laser. *FEBS Lett.* 1984;175(1):95-99.
9. Corral-Baqués MI, Rivera MM, Rigau T, Rodríguez-Gil JE, Rigau J. The effect of low-level laser irradiation on dog spermatozoa motility is dependent on laser output power. *Lasers Med Sci.* 2009;24(5):703-713.
10. Janett F, Stump R, Burger D, Thun R. Suppression of testicular function and sexual behavior by vaccination against GnRH (Equity) in the adult stallion. *Anim Reprod Sci.* 2009;115(1-4): 88-102.
11. O'Hara L, Hanrahan JP, Richardson L, et al. Effect of storage duration, storage temperature, and diluents on the viability and fertility of fresh ram sperm. *Theriogenology.* 2010;73(4):541-549.
12. Hafez B. *Reproduction in Farm Animals*, 7th ed. Hoboken: Wiley-Blackwell; 2000:385.
13. Triwulaningsih E, Situmorang P, Sugiarti T, Sianturi RG, Kusuman-ingrum DA. Effect of glutathione addition to the sperm diluents medium on quality of bovine chilled semen. *Indones J Agric.* 2010;3(1):60-65.
14. Yan JG, Agresti M, Bruce T, Yan YH, Granlund A, Matloub HS. Effects of cellular phone emissions on sperm motility in rats. *Fertil Steril.* 2007;88(4):957-964.
15. Nur Z, Zik B, Ustuner B, Sagirkaya H, Ozguden CG. Effects of different cryoprotective agents on ram sperm morphology and DNA integrity. *Theriogenology.* 2010;73(9):1267-1275.
16. Matás C, Sansegundo M, Ruiz S. Sperm treatment affects capacitation parameters and penetration ability of ejaculated and epididymal boar spermatozoa. *Theriogenology.* 2010;74(8): 1327-1340.
17. Peng X, Li F, Li S, Zhu Y. Expression of a mitochondrial gene or fh79 from the CMS-HongLian rice inhibits *Saccharomyces cerevisiae* growth and causes excessive ROS accumulation and decrease in ATP. *Biotechnol Lett.* 2009;31(3):409-414.
18. Kim S, Agca Y. Changes in rat spermatozoa function after cooling, cryopreservation and centrifugation processes. *Cryobiology.* 2012;65(3):215-223.

19. Li HY, Zhang H. Proteome analysis for profiling infertility markers in male mouse sperm after carbon ion radiation. *Toxicology*. 2013;306:85-92.
20. He Y, Wang K, Zhao X, Zhang Y, Ma Y, Hu J. Differential proteome association study of freeze-thaw damage in ram sperm. *Cryobiology*. 2016;72(1):60-68.
21. Xu W, Hu H, Wang Z, et al. Proteomic characteristics of spermatozoa in normozoospermic patients with infertility. *J Proteomics*. 2012;75(17):5426-5436.
22. Shojaei Saadi HA, van Riemsdijk E, Dance AL, Rajamanickam GD, Kastelic JP, Thundathil JC. Proteins associated with critical sperm functions and sperm head shape are differentially expressed in morphologically abnormal bovine sperm induced by scrotal insulation. *J Proteomics*. 2013;82:64-80.
23. Li HY, Zhang H, Xie Y, et al. Proteomic analysis for testis of mice exposed to carbon ion radiation. *Mutat Res*. 2013;755(2):148-155.
24. Li HY, He YX, Yan JW, Zhao QY, Di CX, Zhang H. Comparative proteomics reveals the underlying toxicological mechanism of low sperm motility induced by iron ion radiation in mice. *Reprod Toxicol*. 2016;65:148-158.
25. du Plessis SS, Agarwal A, Mohanty G, van der Linde M. Oxidative phosphorylation versus glycolysis: what fuel do spermatozoa use? *Asian J Androl*. 2015;17(2):230-235.
26. Aitken RJ, Curry BJ. Redox regulation of human sperm function: from the physiological control of sperm capacitation to the etiology of infertility and DNA damage in the germ line. *Antioxid Redox Signal*. 2011;14(3):367-381.
27. Opuwari CS, Henkel RR. An update on oxidative damage to spermatozoa and oocytes. *Biomed Res Int*. 2016;2016:9540142.
28. Hering DM, Lecewicz M, Kordan W, Kamiński S. Association between ETFA genotype and activity of superoxide dismutase, catalase and glutathione peroxidase in cryopreserved sperm of holstein–friesian bulls. *Reprod Domest Anim*. 2015;50(1):168-171.
29. Völgyi K, Gulyásky P, Háden K, et al. Synaptic mitochondria: a brain mitochondria cluster with a specific proteome. *J Proteomics*. 2015;120:142-157.
30. Wajner M, Amaral AU. Mitochondrial dysfunction in fatty acid oxidation disorders: insights from human and animal studies. *Biosci Rep*. 2015;36(1): e00281.
31. Nair P, Hamzeh AR, Mohamed M, Malik EM, Al-Ali MT, Bastaki F. Novel ECHS1 mutation in an Emirati neonate with severe metabolic acidosis. *Metab Brain Dis*. 2016;31(5):1189-1192.
32. Watmough NJ, Frerman FE. The electron transfer flavoprotein: ubiquinone oxidoreductases. *Biochim Biophys Acta*. 2010;1797(12):1910-1916.
33. Chen X, Zhu H, Hu C, et al. Identification of differentially expressed proteins in fresh and frozen-thawed boar spermatozoa by iTRAQ-coupled 2D LC-MS/MS. *Reproduction*. 2014;147(3):321-330.
34. Onishi M, Yasunaga T, Tanaka H, Nishimune Y, Nozaki M. Gene structure and evolution of testicular haploid germ cell-specific genes, *Oxct2a* and *Oxct2b*. *Genomics*. 2004;83(4):647-657.
35. Zhang S, Xie C. The role of OXCT1 in the pathogenesis of cancer as a rate-limiting enzyme of ketone body metabolism. *Life Sci*. 2017;183:110-115.
36. van Weeghel M, te Brinke H, van Lenthe H, et al. Functional redundancy of mitochondrial enoyl-CoA isomerases in the oxidation of unsaturated fatty acids. *FASEB J*. 2012;26(10):4316-4326.
37. Falk MJ, Gai X, Shigematsu M, et al. A novel HSD17B10 mutation impairing the activities of the mitochondrial RNase P complex causes X-linked intractable epilepsy and neurodevelopmental regression. *RNA Biol*. 2016;13(5):477-485.
38. Pantaleo MA, Astolfi A, Urbini M, et al; GIST Study Group. Analysis of all subunits, SDHA, SDHB, SDHC, SDHD, of the succinate dehydrogenase complex in KIT/PDGFRα wild-type GIST. *Eur J Hum Genet*. 2014;22(1):32-39.
39. Kwon WS, Rahman MS, Lee JS, et al. A comprehensive proteomic approach to identifying capacitation related proteins in boar spermatozoa. *BMC Genomics*. 2014;15:897.
40. Huang YL, Fu Q, Yang L, et al. Differences between high- and low-motility buffalo sperm identified by comparative proteomics. *Reprod Domest Anim*. 2015;50(3):443-451.
41. Ferramosca A, Conte A, Moscatelli N, Zara V. A high-fat diet negatively affects rat sperm mitochondrial respiration. *Andrology*. 2016;4(3):520-525.
42. Martínez-Heredia J, de Mateo S, Vidal-Taboada JM, Ballescà JL, Oliva R. Identification of proteomic differences in asthenozoospermic sperm samples. *Hum Reprod*. 2008;23(4):783-791.
43. Amos L. The tektin family of microtubule-stabilizing proteins. *Genome Biol*. 2008;9(7):229.
44. Xu K, Wen M, Duan W, et al. Comparative analysis of testis transcriptomes from triploid and fertile diploid cyprinid fish. *Biol Reprod*. 2015;92(4):95.
45. Chen Y, Su Z. Reveal genes functionally associated with ACADS by a network study. *Gene*. 2015;569(2):294-302.